SUPPORTING INFORMATION FOR

# Covalent Rpn13-binding inhibitors for the treatment of Ovarian Cancer

Ravi K. Anchoori[1], Rosie Jiang[2], Shiwen Peng[2], Ruey-shyang Soong[2,4], Aliyah Algethami[2], Michelle A Rudek[1], Nicole Anders[1], Chien-Fu Hung[2], Xiang Chen[5], Xiuxiu Lu[5], Olumide Kayode[5], Marzena Dyba[6,7], Kylie J. Walters[5] and Richard B.S. Roden*[1,2,3]

Departments of Oncology[1], Pathology[2], Gynecology and Obstetrics[3], The Johns Hopkins University, Baltimore, MD 21231, USA; Department of General Surgery[4], Chang Gung Memorial Hospital at Keelung, Keelung City, Taiwan 204, ROC; Chang Gung University, College of Medicine, Taoyuan, Taiwan 33302, ROC; Protein Processing Section[5], Biophysics Resource[6], Basic Science Program, Leidos Biomedical Research, Inc.[7], Structural Biophysics Laboratory, Center for Cancer Research, National Cancer Institute, Frederick, MD 21702, USA.

***Corresponding author:** Richard Roden, Department of Pathology, The Johns Hopkins University, Room 308, CRB2, 1550 Orleans St, Baltimore, MD 21231 USA

Tel: 410 502 5161

Fax: 443 287 4295

Email: roden@jhmi.edu

## SUPPLEMENTARY FIGURES

### Figure S1. Identification of RPN13 as a 42 kDa cellular target of RA183B

(**A**) Untreated and RA183B-treated (1 µM, 45 min, 4 °C) SKOV3 lysate was incubated overnight with streptavidin-coated magnetic beads. The beads were separated with a magnet, washed and the bound proteins eluted with 10 mM EDTA pH 8.2 and 95% formamide for 10 min at 90 °C. The input lysate (input), supernatant after bead extraction (SN) and eluates from beads (beads) were subjected to Western blot with RPN13-specific mouse monoclonal antibody. (**B**) Samples in (A) were rerun on SDS-PAGE, transferred to PVDF membrane and probed with HRP-streptavidin. (**C**) Untreated and RA183B-treated (1 µM, 45 min, 4 °C) HeLa cell lysate was incubated overnight with streptavidin-coated Dynabeads. The beads were separated magnetically, washed and the bound proteins eluted with 10 mM EDTA pH 8.2 and 95% formamide for 10 min at 90 °C. The eluates were subjected to Western blot with RPN13-specific mouse monoclonal antibody. (**D, E**) HeLa cells were transfected with siRNA for *ADRM1* or control siRNA and incubated for 48 hours. Cell lysates were then prepared and one portion subjected to Western blot analysis for RPN13 to demonstrate the efficacy of the knockdown (**D**). Another portion of each lysate was probed with HRP-Streptavidin (**E**).

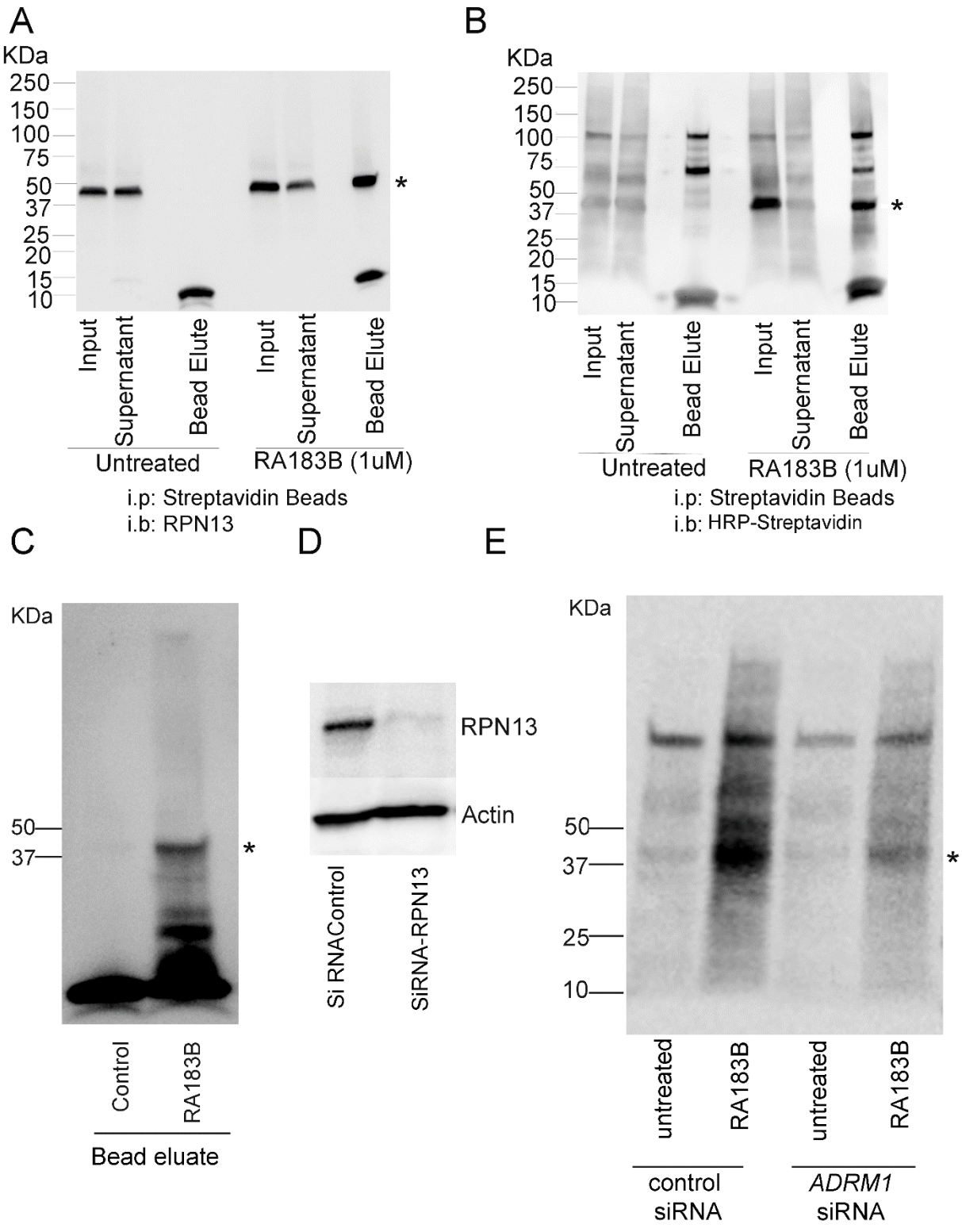
A
KDa
250
150
100
75
50
37
25
20
15
10
*
Input
Supernatant
Bead Elute
Input
Supernatant
Bead Elute
Untreated
RA183B (1uM)
i.p: Streptavidin Beads
i.b: RPN13
B
KDa
250
150
100
75
50
37
25
20
15
10
*
Input
Supernatant
Bead Elute
Input
Supernatant
Bead Elute
Untreated
RA183B (1uM)
i.p: Streptavidin Beads
i.b: HRP-Streptavidin
C
KDa
50
37
*
Control
RA183B
Bead eluate
D
RPN13
Actin
Si RNAControl
SiRNA-RPN13
E
KDa
50
37
25
10
*
untreated
RA183B
untreated
RA183B
control siRNA
ADRM1 siRNA

**Figure S2. RPN13 Pru~RA183 structure calculations yield three clusters**

(**A**) ($^{1}$H, $^{15}$N) HSQC spectra of $^{15}$N-labeled RPN13 Pru domain with C88 replaced with alanine without (black) and with 10-fold molar excess of RA183 added, followed by sample dialysis to remove excess and labile RA183 (orange). (**B**) ($^{1}$H, $^{15}$N) HSQC spectra of $^{15}$N-labeled RPN13 Pru domain with C60, C80 and C121 replaced with alanine without (black) and with 10-fold molar excess of RA183 added, followed by dialysis for removal of excess and labile RA183 (orange). (**C**) RPN13 Pru~RA183 structures were sorted into three clusters by using a 1.5 Å cut-off criterion with structural statistics as summarized in the table. $E_{inter}$, intermolecular binding energy; $E_{vdw}$, van der Waals energy; $E_{elec}$, electrostatic energy; BSA, buried surface area; RMSD, root mean square deviation for backbone atoms to the cluster average structure. (**D**) Ribbon diagrams for the lowest energy model structure from cluster 2 and 3 of RPN13~RA183 with coloring identical to that of Figure 2E. (**E**) Expanded views of lowest energy model structure for RPN13 Pru~RA183 (left panel) and RPN13 Pru~RA190 (right panel) complexes to illustrate interactions at the contact surface with key amino acids, RA183 or RA190 displayed and labeled. (**F**) Expanded view of the lowest energy model structure from cluster 2 for RPN13 Pru~RA183 illustrating interactions at the contact surface with key amino acids and RA183 displayed and labeled. (**G**) Superimposed lowest energy model structures from cluster 1 and 3 with RA183 colored in blue or green respectively.

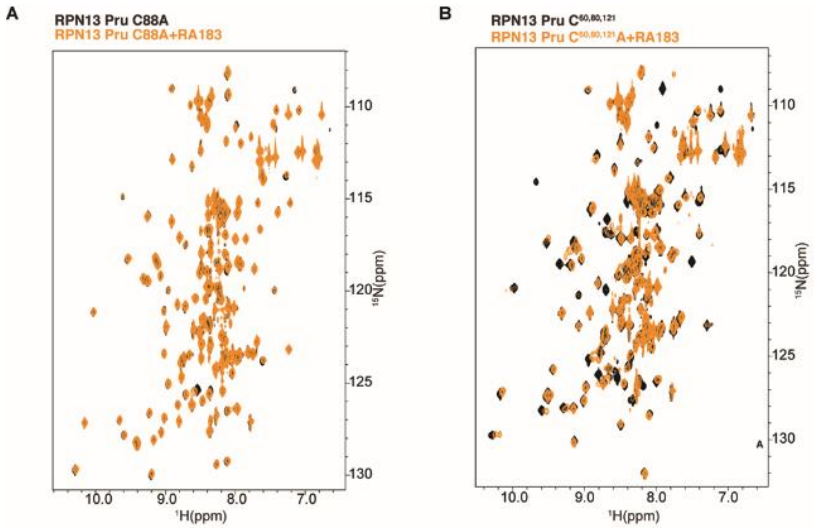


C

| Cluster No. | Number of Structures | Haddock score | RMSD | $E_{inter}$ | $E_{vdw}$ | $E_{elec}$ | BSA |
|---|---|---|---|---|---|---|---|
| 1 | 141 | 74.11±4.93 | 0.72±0.14 | 199.97±27.55 | 70.51±2.95 | -26.05±8.24 | 675.64±29.20 |
| 2 | 67 | 75.00±5.51 | 0.54±0.11 | 212.11±29.71 | 69.83±3.32 | -20.48±6.41 | 650.66±28.61 |
| 3 | 20 | 77.20±4.88 | 0.50±0.13 | 229.67±26.39 | 71.46±2.64 | -9.61±5.74 | 584.06±27.24 |

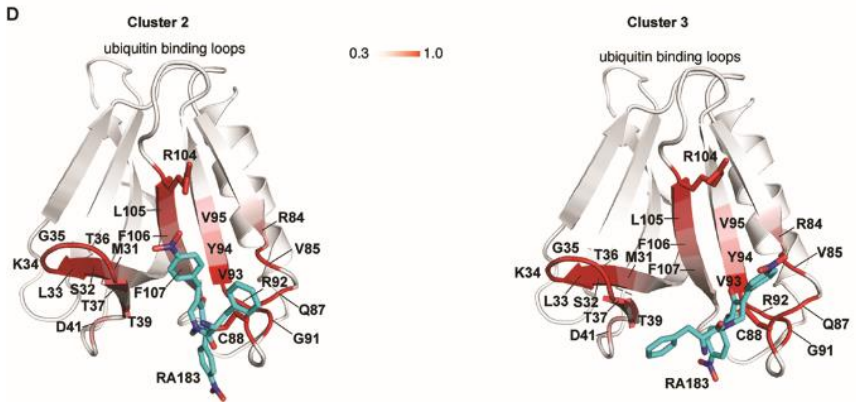


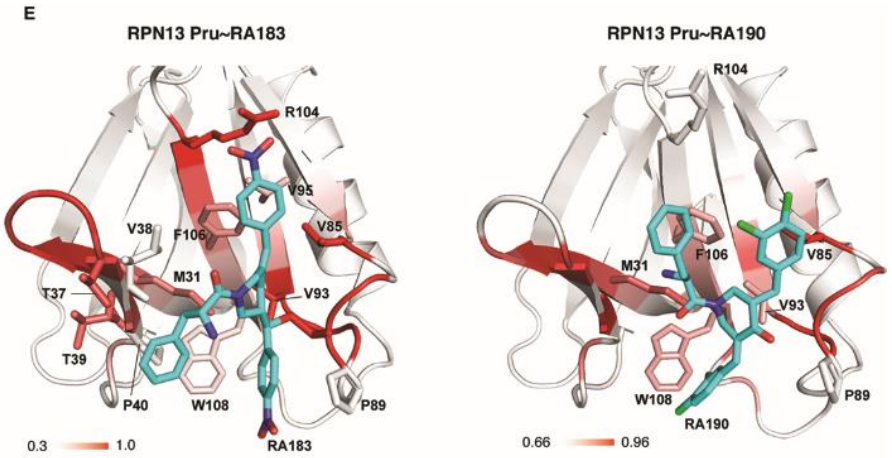


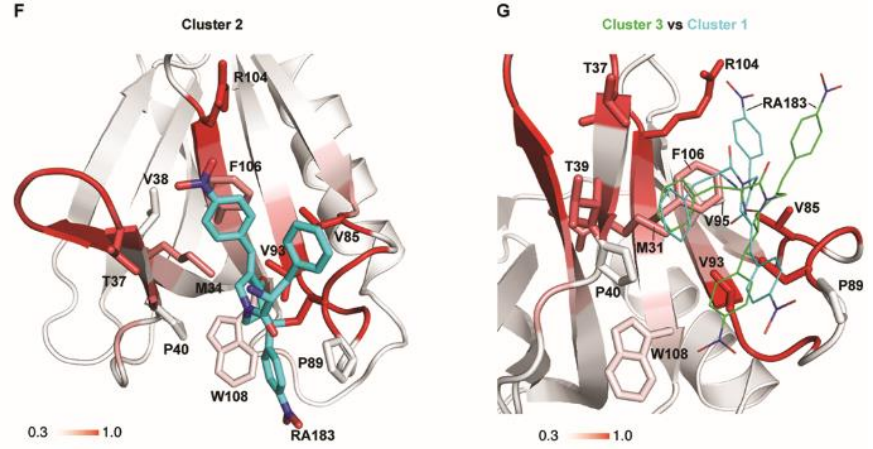

**Figure S3. Analysis of RA183 binding to RPN13 in cell lysates.**

(**A**) We compared the effectiveness of pre-incubation of SKOV3 cell lysate with b-AP15 or RA9 to compete with RA183B binding to RPN13 following separation by SDS-PAGE, transfer to a membrane and detection with HRP-Streptavidin. The 20S CP inhibitor bortezomib was used as a negative control. Detergent lysate extracted from 5 x $10^6$ SKOV3 cells was pretreated with DMSO (control), or 10 µM each of RA9, b-AP15, RA190, RA183 or bortezomib for 45 min at 37 °C; then 1 µM RA183B was added to each and incubated for a further 45 min. After labeling equal aliquots were separated by SDS-PAGE, transferred to PVDF membrane and probed with HRP-streptavidin. When the lysate was pretreated with b-AP15, RA190 or RA183 and then labeled with RA183B, each reduced RA183B labeling of the 42 kDa cellular target, and RA183 was the most potent. RA9 and bortezomib had minimal impact on labeling at 42 kDa. (**B**) Since RA183 binds to RPN13 more potently than RA190, we next compared the ability of RA183, RA190 and b-AP15 to compete with RA190B for binding to its 42 kDa target in cell lysate. 293TT cell lysate was pretreated with RA183, RA190 or b-AP15 (1 µM, 45 min at 4 °C) and then labelled with 20 µM RA190B for 45 min at 4 °C. Labelling was assessed as in (A). RA183 out-competed RA190B for binding to its 42 kDa target in cell lysate more strongly than did b-AP15), and a second much weaker band at 37 kDa (consistent with UCH37 that is bound by RA190 in vitro [1]. (**C**) To examine whether b-AP15 could compete with binding of RA183B to RPN13, SKOV3 lysate was pretreated with DMSO (control), b-AP15, or RA183 at 0.5-50 µM and then labeled with RA183B and subjected to SDS-PAGE, transferred to a membrane and probed with HRP-Streptavidin. Less effective competition with RA183B binding to RPN13 was observed using b-AP15 as compared to RA183. (**D**) SKOV3 lysate was pretreated with DMSO (control) or VLX1570 at the indicated concentrations for 45 min at 4 °C and then labeled with RA183B for 45 min at 4 °C. Labelling was assessed as in (A).

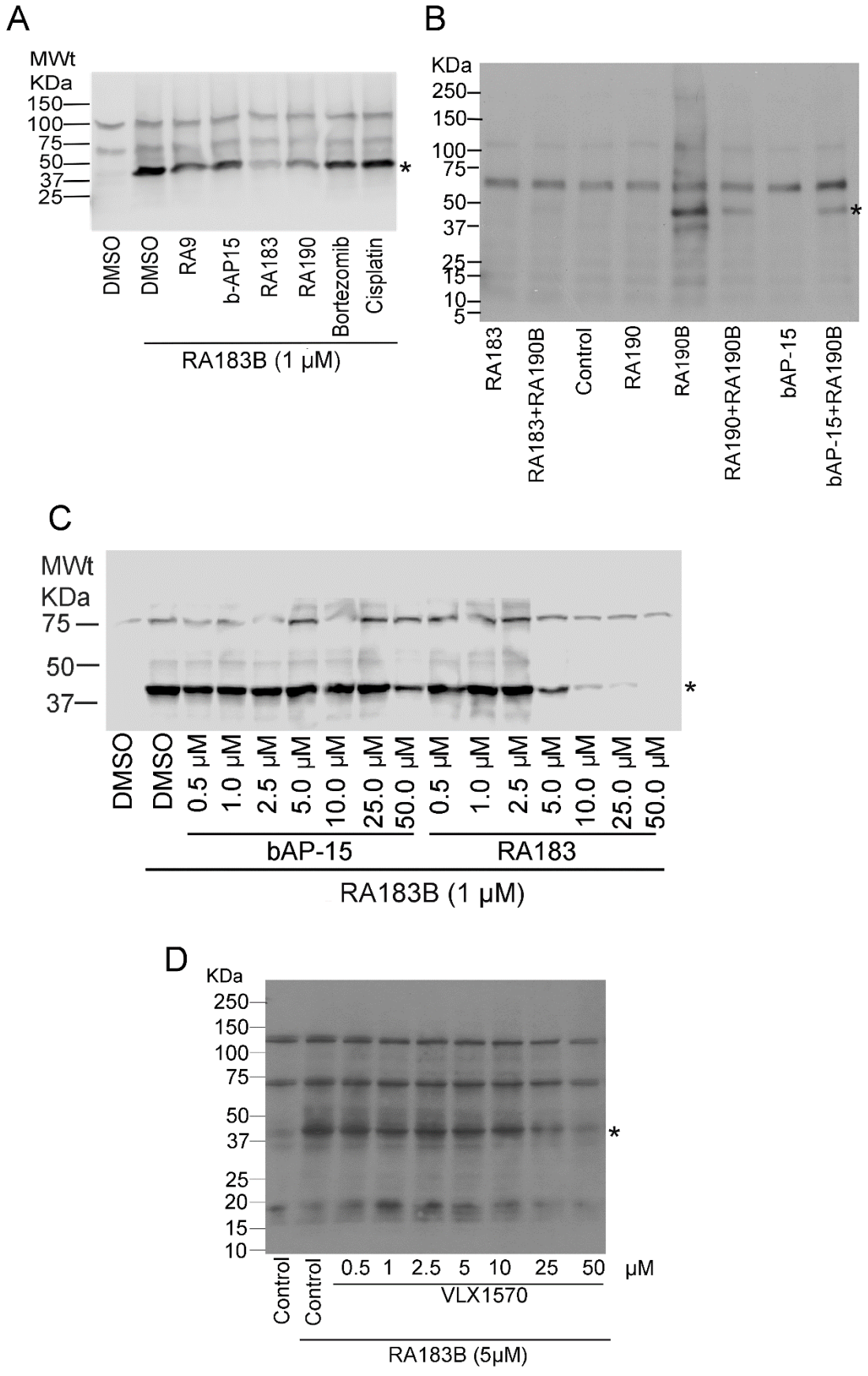
A
MWt
KDa
150
100
75
50
37
25
*
DMSO
DMSO
RA9
b-AP15
RA183
RA190
Bortezomib
Cisplatin
RA183B (1 μM)
B
KDa
250
150
100
75
50
37
25
15
10
5
*
RA183
RA183+RA190B
Control
RA190
RA190B
RA190+RA190B
bAP-15
bAP-15+RA190B
C
MWt
KDa
75
50
37
*
DMSO
DMSO
0.5 μM
1.0 μM
2.5 μM
5.0 μM
10.0 μM
25.0 μM
50.0 μM
0.5 μM
1.0 μM
2.5 μM
5.0 μM
10.0 μM
25.0 μM
50.0 μM
bAP-15
RA183
RA183B (1 μM)
D
KDa
250
150
100
75
50
37
25
20
15
10
*
Control
Control
0.5 1 2.5 5 10 25 50 μM
VLX1570
RA183B (5μM)

**Figure S4. RPN13 Pru domain interacts with b-AP15.**

(**A**) ($^{1}$H, $^{15}$N) HSQC spectra of $^{15}$N-labeled RPN13 Pru domain without (black) and with 10-fold molar excess b-AP15 and following dialysis to remove excess and labile compound (orange). Signals affected by b-AP15 are labeled. (**B**) Normalized peak intensity attenuation ($\Delta$) of RPN13 Pru domain backbone amide groups upon binding b-AP15. The dashed line indicates one SD above average. Unassigned, overlapping, or proline groups are excluded from this analysis and indicated (*). Signal loss was observed for several RPN13 Pru residues, including Cys88, with a pattern reminiscent of the effect of RA183 (**Figure 2A**) or RA190 [2] (**C**) LC-MS experiment for b-AP15-exposed $^{15}$N-labeled RPN13 Pru domain; this sample is identical to the one used in (A). Unmodified $^{15}$N-labeled Rpn13 was present (17222 Da) with an additional species at a molecular weight shifted by 418.2 Da. The expected molecular weight shift caused by b-AP15 attachment is 419.4 Da. (**D**) Ribbon diagram of RPN13 Pru with amino acids attenuated in (A) indicated by a red gradient as illustrated in the figure legend and based on the quantified data in (B). The b-AP15-bound RPN13 Pru (A) yielded weaker signals compared to RA183-bound RPN13 Pru by NMR (**Figure 2A**). When we quantified the observed signal attenuation of RPN13 Pru signals caused by b-AP15 (B) we observed that the most impacted amino acids reside on the surface opposite to the ubiquitin-binding loops, as previously seen for RA183 (**Figure 2F, G**) and RA190 [2].

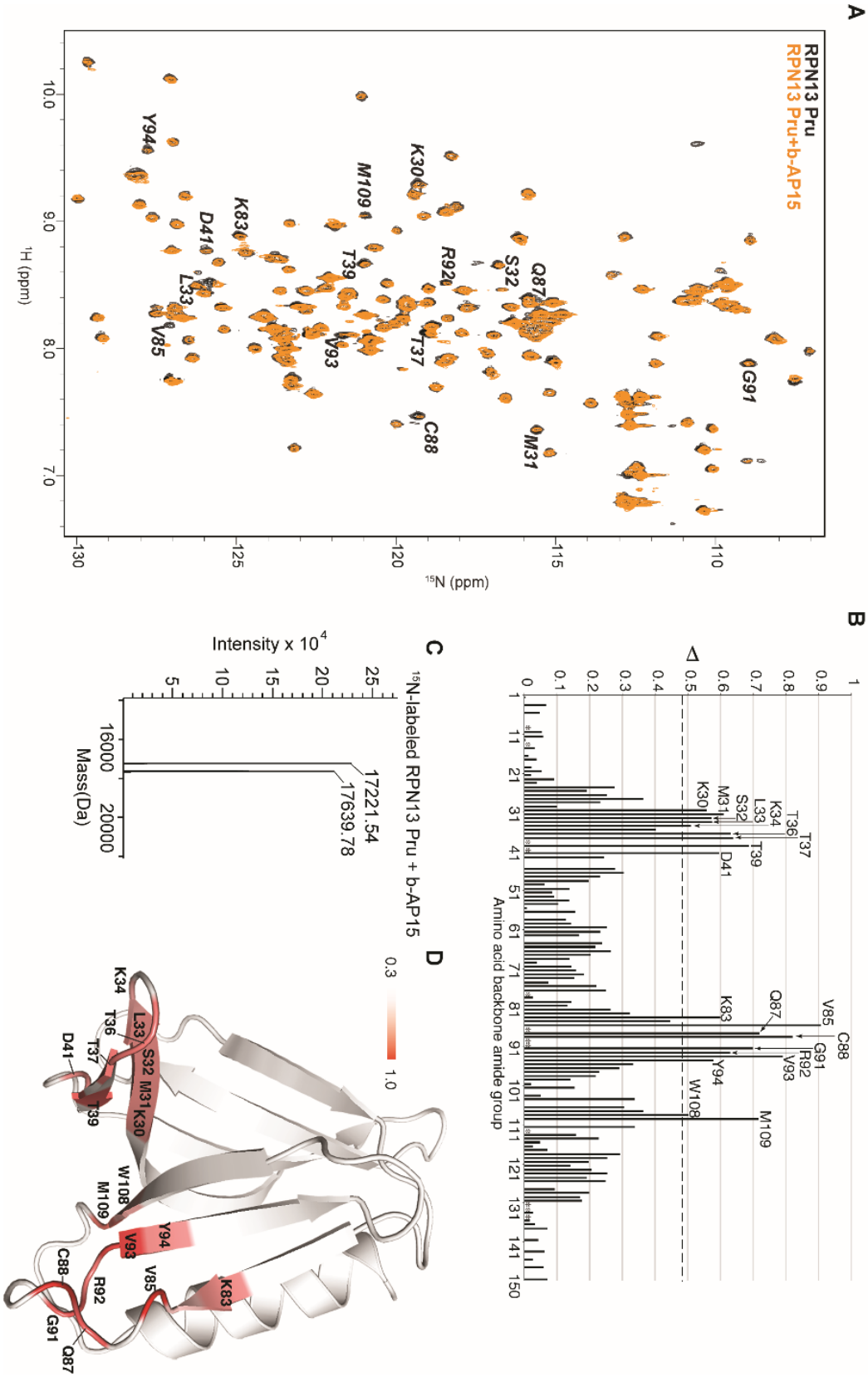
A
RPN13 Pru
RPN13 Pru+b-AP15
$^{15}$N (ppm)
$^{1}$H (ppm)
B
Δ
Amino acid backbone amide group
C
$^{15}$N-labeled RPN13 Pru + b-AP15
Intensity x $10^4$
Mass(Da)
17221.54
17639.78
D
0.3
1.0

**Figure S5. Impact of RA183 on 19S RP DUBs and 20S CP**

(**A**) Purified 19S RP was incubated with RA183, RA190 or the known DUB inhibitors b-AP15 and HA-UbVS. The DUB activity of the 19S RP was then examined by addition of the substrate Ub-AMC, and fluorescence was measured to follow Ub-AMC cleavage. (**B**) To determine whether RA183 binds the 19S RP DUBs USP14 and UCH37, OV2008 cell lysate was pre-treated with RA183 (0, 2.5, 5, 10 or 25 μM) for 45 min at 4 °C and then labeled with 2μM HA-UbVS. The lysates were then analyzed by Western blot for USP14 (top panel) or UCH37 (bottom panel). Tubulin was used as loading control. (**C**) 2 μM UCH37 with 50 μM RA183 incubation for 2 hours and sample subjected to LC-MS analysis to detect the formation of RA183 adducts. (**D-F**) We also examined whether RA183 inhibits proteasome 20S CP by measuring *in vitro* the cleavage of fluorescent substrate corresponding to its chymotryptic, caspase (PGPH) and tryptic-like activities. Purified 20S proteasomes were treated for 30 min with 1 μM RA183 or 1 μM bortezomib prior to the addition of the specific fluorogenic substrate for chymotryptic (**D**), tryptic (**E**), PGPH (**F**) proteasome capacities. Mean ± SD fluorescence associated with AMC released from the substrate was measured at 45 min.

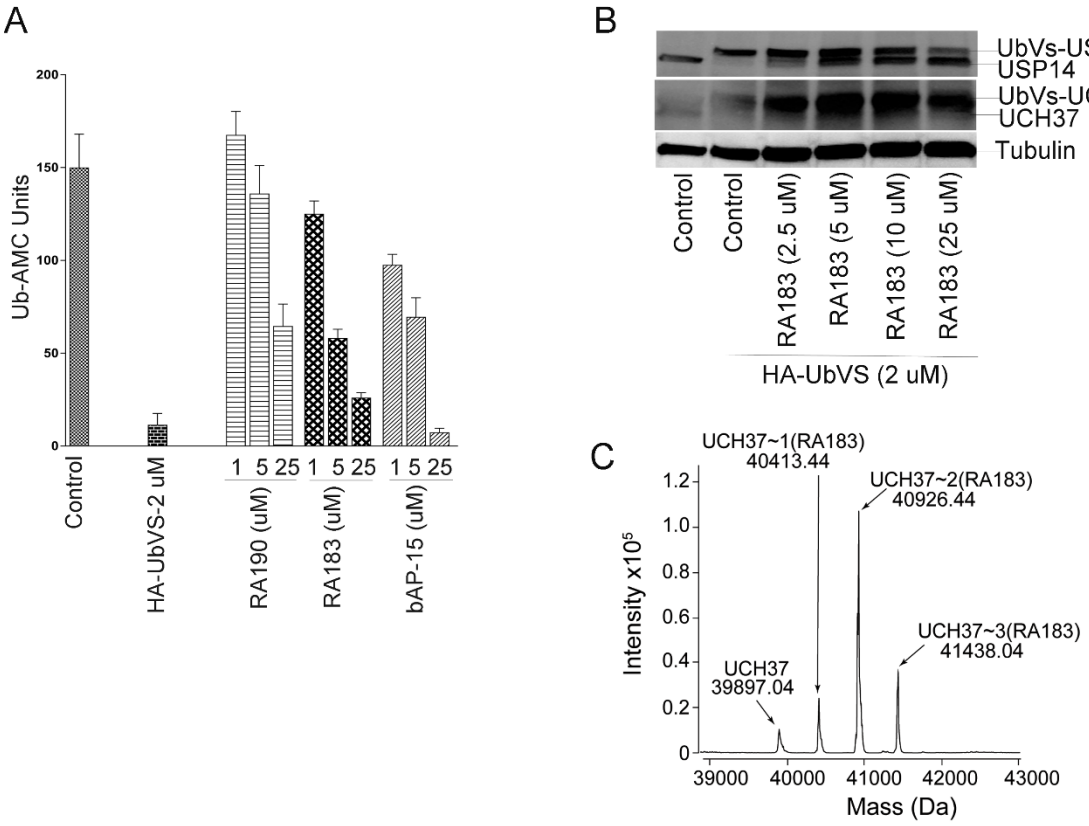
A
Ub-AMC Units
200
150
100
50
0
Control
HA-UbVS-2 uM
1 5 25 1 5 25 1 5 25
RA190 (uM)
RA183 (uM)
bAP-15 (uM)
B
UbVs-USP14
USP14
UbVs-UCH37
UCH37
Tubulin
Control
Control
RA183 (2.5 uM)
RA183 (5 uM)
RA183 (10 uM)
RA183 (25 uM)
HA-UbVS (2 uM)
C
UCH37~1(RA183)
40413.44
UCH37~2(RA183)
40926.44
UCH37~3(RA183)
41438.04
UCH37
39897.04
Intensity x10^5
1.2
1.0
0.8
0.6
0.4
0.2
0
39000
40000
41000
42000
43000
Mass (Da)

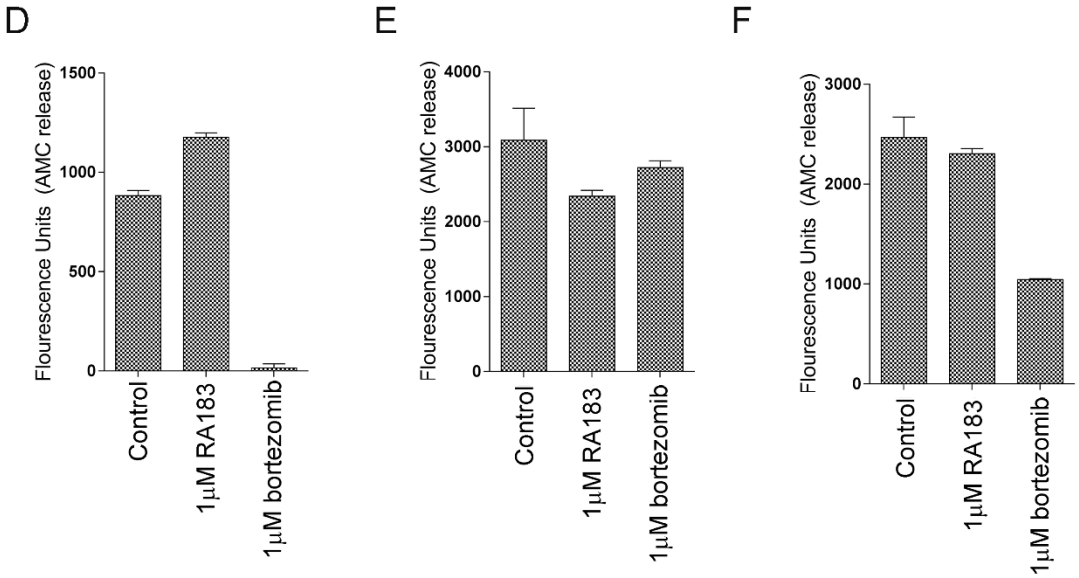
D
Flourescence Units (AMC release)
1500
1000
500
0
Control
1μM RA183
1μM bortezomib
E
Flourescence Units (AMC release)
4000
3000
2000
1000
0
Control
1μM RA183
1μM bortezomib
F
Flourescence Units (AMC release)
3000
2000
1000
0
Control
1μM RA183
1μM bortezomib

**Figure S6. In Vitro Microsomal Stability of RA183 and RA190**

RA183 stability and metabolism studies were conducted in a 0.5M sodium-potassium phosphate buffer (pH 7.4) containing 20 mg/mL of either human or mouse liver microsomes, NADPH-generating system A and B, and 10 mM of RA183 in a final volume of 500 µL. Negative controls were performed without NADPH-generating system to control for native enzyme activities. Incubations were performed in duplicate in glass tubes maintained at 37 °C in a shaker bath. Reactions were terminated immediately or after 0.5 or 1 hr by taking 20 µL of the reaction mixture and adding 1 mL of acetonitrile, followed by vortex-mixing then centrifugation for 10 min at 1430 *x g*. A 10 µL aliquot of the supernatant was injected onto the UPLC instrument for qualitative analysis using a temperature-controlled autosampling device operating at 5°C.

| | | Human Microsomes | | | Mouse Microsomes | | |
|---|---|---|---|---|---|---|---|
| Sample time (min) | Drug | With (+) or Without (-) NADPH | Average Ratio | % of area ratio compared time 0 | With (+) or Without (-) NADPH | Average Ratio | % of area ratio compared time 0 |
| 0 | RA 190 | - | 2.56 | 100 | - | 2.27 | 100 |
| 30 | RA 190 | - | 1.57 | 61 | - | 1.54 | 68 |
| 60 | RA 190 | - | 1.41 | 55 | - | 1.47 | 65 |
| 0 | RA 190 | + | 2.37 | 100 | + | 2.71 | 100 |
| 30 | RA 190 | + | 1.62 | 69 | + | 1.93 | 71 |
| 60 | RA 190 | + | 1.40 | 59 | + | 1.78 | 66 |

| | | Human Microsomes | | | Mouse Microsomes | | |
|---|---|---|---|---|---|---|---|
| Sample time (min) | Drug | With (+) or Without (-) NADPH | Average Ratio | % of area ratio compared time 0 | With (+) or Without (-) NADPH | Average Ratio | % of area ratio compared time 0 |
| 0 | RA 183 | - | 1.56 | 100 | - | 1.51 | 100 |
| 30 | RA 183 | - | 1.17 | 75 | - | 1.11 | 74 |
| 60 | RA 183 | - | 0.97 | 62 | - | 0.99 | 66 |
| 0 | RA 183 | + | 1.76 | 100 | + | 1.64 | 100 |
| 30 | RA 183 | + | 0.22 | 13 | + | 0.93 | 57 |
| 60 | RA 183 | + | 0.05 | 3 | + | 0.61 | 37 |

**Figure S7. Metabolite analysis of RA183**

Chromatographic analysis was performed using a Waters Acquity ™ UItra Performance LC. Separation of the analyte from potentially interfering material and metabolites was achieved at ambient temperature using Agilent Zorbax XDB C18 column (50 x 2.1 mm i.d.) with a 3.5 µm particle size. (Santa Clara, CA). The mobile phase used for the chromatographic separation was composed of 0.1% (v/v) formic acid in water (mobile phase A) and 0.1% (v/v) formic acid in acetonitrile (mobile phase B) with a flow rate of 0.3 mL/min. The initial mobile phase composition was 80% mobile phase A and 20% mobile phase B. From 0 to 7 min, mobile phase B was increased linearly from 20% to 50%. From 7 to 8 min, mobile phase B was increased linearly from 50% to 100% and maintained until 9 min. From 9.0 to 9.1 min, the gradient decreased to 20% mobile phase B and the conditions were maintained until 12 min to re-equilibrate the column for the next injection. The column effluent was monitored using an AB Sciex QTrap ™ 5500. The instrument was equipped with an electrospray interface, operated in a positive mode and controlled by the Analyst v1.6 software. For the stability study, the mass spectrometer was programmed to monitor the following MRM transition 513.1 → 120.1 for RA183. Results were assessed qualitatively comparing the average area ratio of RA183 at 0hr to area ratio at 0.5 hr and 1 hr for both mouse and human liver microsomes. While the LC method remained the same, the following mass spectrometer experiments were performed to help determine the metabolites and their structures: full scan, MRM (multiple reaction monitoring), and precursor and neutral loss of various Q3 fragments. Possible metabolites were identified having a signal intensity greater than 3 times the intensity of the control sample. The methods and results were processed using LightSight v2.3 software.

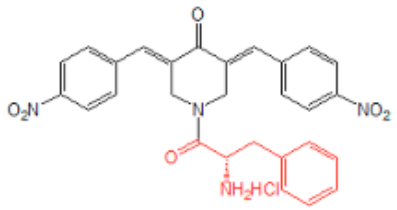


RA183 (m/z : 513)

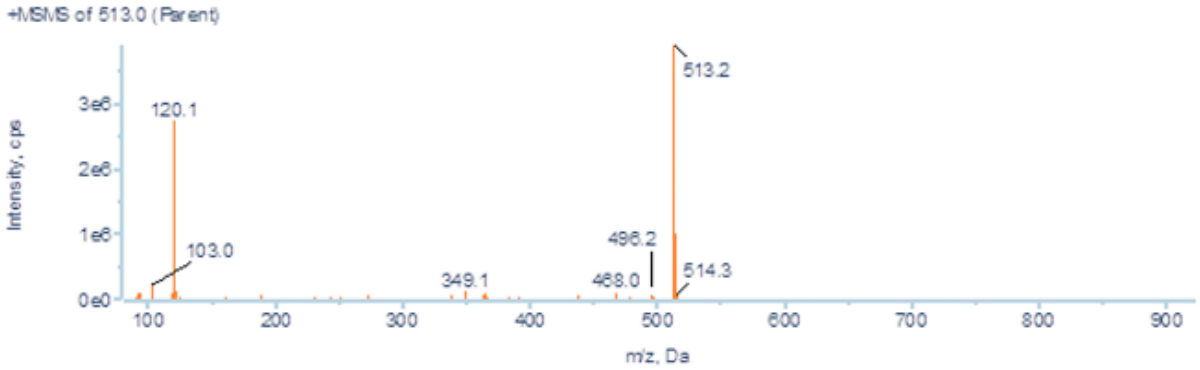


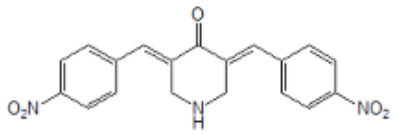


Proposed metabolite for RA183 (m/z : 366)

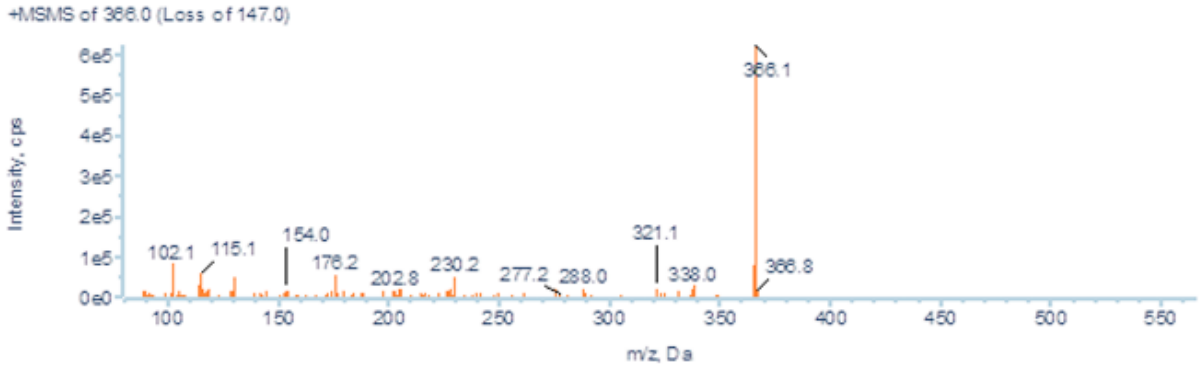

**Table S1. Anti-proliferative activity of RA-series compounds against cancer and immortalized keratinocyte lines as determined by MTT assay. A.** $IC_{50}$ values were determined in triplicate and are presented in μM. TNBC = Triple Negative Breast Cancer.

| | | IC50 (μM) | | |
|---|---|---|---|---|
| Name | Cancer Type | RA183 | RA190 | b-AP15 |
| OVCAR3 | Ovarian, serous | 0.078 | 0.12 | 0.35 |
| Kuramochi | Ovarian, undifferentiated | 1.012 | 1.065 | 2.690 |
| SKOV3 | Ovarian, epithelial | 0.054 | 0.073 | 0.236 |
| TOV21G | Ovarian, epithelial | 0.044 | 0.083 | 0.179 |
| PE014 | Ovarian, serous | 0.669 | 0.628 | |
| OAW42 | Ovarian, serous | 0.134 | 0.257 | |
| ES2 | Ovarian, clear cell | 0.075 | 0.115 | |
| A2780 | Ovarian, endometrioid | 0.161 | 0.139 | |
| COV318 | Ovarian, serous | 0.838 | 0.3 | |
| COLO704 | Ovarian, high-grade serous carcinoma | 1.25 | 1.25 | |
| MDA-MB-231 | Basal B, TNBC | 0.124 | 0.134 | 0.436 |
| HS578T | Basal B, TNBC | 0.089 | 0.078 | |
| HCC1806 | Basal A, TNBC | 0.044 | 0.052 | |
| T47D | Breast, luminal A | 1.09 | 0.48 | 1.83 |
| BT549 | Basal B, TNBC | 0.213 | 0.212 | |
| MCF10A | Basal B, TNBC | 0.192 | 0.184 | |
| MCF7 | Breast, luminal A | 0.5 | 0.32 | 1.188 |
| MM1S | Multiple myeloma | 0.04 | 0.07 | |
| NCI-H929 | Multiple myeloma | 0.04 | 0.04 | |
| U266 | Multiple myeloma | 0.175 | 0.175 | |
| ANBL6 | Multiple myeloma | 0.058 | | |
| ANBL6-V10R | Multiple myeloma | 0.103 | | |
| RPMI | Multiple myeloma | 0.088 | | |
| RPMI-V10R | Multiple myeloma | 0.139 | | |
| MiaPaca-2 | Pancreatic | 0.34 | 0.28 | |
| A549 | Lung | 0.209 | 0.236 | |
| HeLa | Cervical | 0.112 | 0.15 | |
| CaSki | Cervical | 0.3 | 0.3 | |
| SiHa | Cervical | 0.263 | 0.75 | |
| ME180 | Cervical | 0.293 | 0.183 | |
| HaCaT | immortalized keratinocyte | >2.5 | >2.5 | |
| HFF | human foreskin fibroblast | >2.5 | >2.5 | |

**BIBLIOGRAPHY FOR SUPPLEMENTARY INFORMATION**

1. Lu, X.; Nowicka, U.; Sridharan, V.; Liu, F.; Randles, L.; Hymel, D.; Dyba, M.; Tarasov, S. G.; Tarasova, N. I.; Zhao, X. Z.; Hamazaki, J.; Murata, S.; Burke, T. R., Jr.; Walters, K. J., Structure of the Rpn13-Rpn2 complex provides insights for Rpn13 and Uch37 as anticancer targets. *Nat Commun* **2017,** *8*, 15540.

2. Anchoori, R. K.; Karanam, B.; Peng, S.; Wang, J. W.; Jiang, R.; Tanno, T.; Orlowski, R. Z.; Matsui, W.; Zhao, M.; Rudek, M. A.; Hung, C. F.; Chen, X.; Walters, K. J.; Roden, R. B., A bis-Benzylidine Piperidone Targeting Proteasome Ubiquitin Receptor RPN13/ADRM1 as a Therapy for Cancer. *Cancer Cell* **2013,** *24* (6), 791-805.